

## Nuclear magnetic properties of $^3\text{He}$ adsorbed on graphite

R. E. Rapp

*Centre de Recherches sur les Très Basses Températures, Centre National de la Recherche Scientifique,  
Boîte Postale 166, 38042 Grenoble CEDEX 9, France*  
and *Instituto de Física, Universidade Federal do Rio de Janeiro, Bloco A, 4º andar, Cidade Universitaria,  
Caixa Postal 68528, Rio de Janeiro 21945, Brazil*

H. Godfrin

*Centre de Recherches sur les Très Basses Températures, Centre National de la Recherche Scientifique,  
Boîte Postale 166, 38042 Grenoble CEDEX 9, France*  
and *Institut Laue-Langevin, Boîte Postale 156, 38042 Grenoble CEDEX 9, France*

(Received 25 June 1992; revised manuscript received 15 December 1992)

Precise measurements are presented for the nuclear susceptibility of  $^3\text{He}$  films adsorbed on exfoliated graphite at millikelvin temperatures as a function of coverage (0.53–1.42 layers). Ferromagnetic Curie-Weiss temperatures are determined above and below the perfectly commensurate coverage. In the incommensurate phase, the effective exchange interactions are found to be much smaller than those determined by heat capacity, suggesting a strong departure from a Heisenberg Hamiltonian description. The evolution of the NMR line shape as a function of coverage disagrees with previous data in the incommensurate phase and around monolayer completion. The dependence of the Curie constant on coverage is consistent with recent neutron-scattering results, suggesting an interpretation of the phase diagram and a modified coverage scale. We also present a description of the techniques developed in our laboratory which allow performing surface physics experiments at millikelvin temperatures.

### I. INTRODUCTION

We report experimental results on the nuclear susceptibility of  $^3\text{He}$  adsorbed on exfoliated graphite in the submonolayer and bilayer regimes at temperatures down to 2.8 mK. Our results on multilayer systems (not presented here) have been described in earlier publications and thesis.<sup>1–4</sup> Our data bring evidence for a different interpretation of the phase diagram suggested by recent neutron-scattering measurements.<sup>5</sup>

Motivated by the growing interest in two-dimensional (2D)  $^3\text{He}$  systems, we also present here a description of the experimental techniques that we developed to extend the field of surface physics to millikelvin and submillikelvin temperatures.

### II. $^3\text{He}$ ADSORBED ON GRAFOIL: THE PHASE DIAGRAM

The main features of the phase diagram of  $^3\text{He}$  adsorbed on Grafoil have been given by specific-heat,<sup>6,7</sup> neutron-scattering,<sup>5,8</sup> and NMR investigations.<sup>10</sup> Measurements on adsorbed  $^4\text{He}$  and  $\text{H}_2$  adsorbed on Grafoil revealed qualitatively similar behavior.<sup>9</sup> At very low densities (below 2% of a monolayer) the  $^3\text{He}$  atoms seem to be localized,<sup>6,11,12</sup> probably trapped in defects of the Grafoil substrate.

At low densities a region of 2D quantum gases has been observed. Specific heat<sup>6,7</sup> and NMR (Refs. 13 and 14) have shown quantum degeneracy effects at temperatures in the range 0.1–1 K. According to recent heat-capacity data<sup>7</sup> the system remains a gas down to presum-

ably the absolute zero; the regime extends up to a coverage of 0.043 atoms/Å<sup>2</sup>.

A commensurate phase<sup>5–11</sup> with a triangular  $\sqrt{3}R$  30° structure occurs at a density  $n_c = 0.06366 \text{ Å}^{-2}$  up to  $T_c \approx 3 \text{ K}$  (second-order phase transition), and extends over a substantial part of the phase diagram. The exact phase boundaries are not known presently, except near  $(n_c, T_c)$ ; these phase boundaries have been extrapolated to zero temperature by Greywall and Bush using heat-capacity data. A coexistence region (commensurate + fluid) is thought to exist (at zero temperature) between  $0.043 \text{ Å}^{-2}$  and  $n_c$ . Between  $0.0595 \text{ Å}^{-2}$  and  $n_c$ , however, the existence of a commensurate phase with vacancies has been suggested.<sup>7</sup> For coverages between  $n_c$  and  $0.070 \text{ Å}^{-2}$ , a coexistence of solidlike commensurate phases would arise<sup>7</sup> as a consequence of the existence of a new commensurate phase at a density of about  $0.073 \text{ Å}^{-2}$ . Another coexistence region, involving this new phase and the incommensurate solid, would then exist<sup>7</sup> between  $0.073$  and  $0.081 \text{ Å}^{-2}$ . The incommensurate phase<sup>5–11</sup> extends from this coverage up to  $0.112 \text{ Å}^{-2}$ , where promotion to the second layer begins. The second layer remains fluid for coverages up to about  $0.16 \text{ Å}^{-2}$ . Compression of the first layer by the second one has been observed by specific heat<sup>6,7</sup> and measured by neutron diffraction.<sup>5–8</sup> The first layer density in the bilayer regime increases from 0.106 to  $0.111 \text{ Å}^{-2}$  as the second layer is progressively completed. The areal densities given here correspond to values from different sources in the literature; they should be taken with care, since they are not defined using a consistent coverage scale, as will be discussed later in this paper.

### III. EXPERIMENTAL SETUP

Nuclear magnetic resonance measurements on adsorbed  $^3\text{He}$  at millikelvin temperatures require a special design of the experimental setup. The main problem is to cool down the substrate to a few mK; further problems arise from the small volume density of spins (1% of bulk  $^3\text{He}$ ), long time constants and poor thermal contact, and the small measuring and noise power allowed.

#### A. The dilution refrigerator

Our dilution refrigerator has exceptional characteristics which were essential for these measurements. It works normally at a flow rate of  $250\ \mu\text{mol}/\text{sec}$ , reaching a minimum temperature of 2.6 mK, in continuous operation. It has an excellent long-term temperature stability due to a careful design, to the large volume of the mixing chamber ( $150\ \text{cm}^3$ ), and to its high cooling power. The refrigerator ( $^3\text{He}$  circulation type) requires 320 l of mixture with 22% of  $^3\text{He}$ . Its pumping system consists of an Alcatel 2060H mechanical pump and a Pfeiffer  $250\ \text{m}^3/\text{h}$  Roots pump which allow a maximum flow rate of  $1\ \text{mmol}/\text{sec}$ . The low-temperature insert has a continuous counterflow heat exchanger and three sintered silver step exchanges. A detailed calculation of the component dimensions is the key of the refrigerator performance.<sup>15</sup>

#### B. The experimental cell

The cell and the mixing chamber (Fig. 1) are made out of plastic (Araldite) to avoid eddy current heating during the NMR measurements. The cell is immersed in the dilute phase inside the mixing chamber, ensuring, according to our experience, subpicowatt heat leaks. It is mounted on a plastic support glued to the plus at the bottom of the mixing chamber. The filling line of the cell passes through this plastic (Araldite) plug; it consists of 80 cm of 1.5-mm (internal diameter) copper-nickel tube up to the  $^4\text{He}$  bath, and of 80 cm of 2.5-mm (i.d.) tube between the bath and the top of the cryostat.

The cell contains in its center a NMR coil wound on an Araldite form, with 38 Grafoil sheets (mass = 3.26 g) sintered on 19 copper foils (thickness  $25\ \mu\text{m}$ ), cut to fill the coil form (diameter 18 mm, length 20 mm) and degassed at  $800^\circ\text{C}$  for 4 h. The graphite-copper bonding procedure is of particular importance, and its description is given in a separate section. The normal to the Grafoil sheets is perpendicular to the magnetic-field direction and also to the axis of the NMR coil. Kapton foils are used for electrical insulation of the Grafoil sheets. The copper foils have ribbon-shaped tails which are screwed (out of the high rf field region) to a copper post. This post passes through a Stycast seal at the top wall of the cell into the mixing chamber where a sintered silver disk ensures thermal contact (surface area  $4\ \text{m}^2$ ). A heater and a carbon resistance thermometer (Speer  $100\ \Omega$ ) are attached to the post. A CMN mutual inductance thermometer is located above the silver disk.

Superconducting wires (Niomax CNA61/05) are used for all electrical connections up to 4.2 K. The NMR coil is connected to a coaxial line made out of copper-nickel

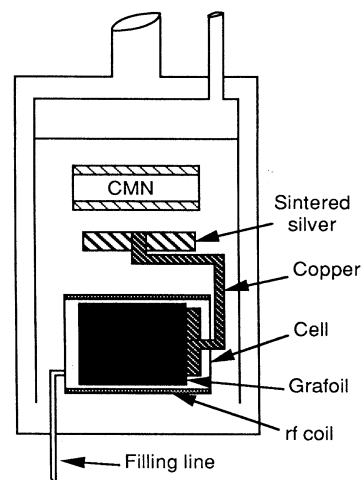


FIG. 1. Mixing chamber of the dilution refrigerator and experimental cell.

tubes; the inner one is partially copper plated to reduce its electrical resistance.

#### C. Graphite-metal bonding

We have developed a method to bond the graphite substrate to a metallic support, which gives excellent thermal and electrical contact. Instead of using copper powder as a bonding agent, as in Ref. 6, we directly bond the graphite onto the metal. This is obtained by pressing the graphite and the metal together in a simple device: two stainless-steel plates held by two stainless-steel screws, with springs or flexible pressure washers. Grafoil spacers are intercalated between the "sample" and the stainless-steel device to protect the sample. The device keeps a reasonable pressure on the graphite-metal "sandwich" during the baking procedure. The assembly is then located in an oven under vacuum (or hydrogen), heated to  $800^\circ\text{C}$  for 4 h, and then cooled to room temperature in a  $^4\text{He}$  atmosphere. The conditions (temperature, device pressure, gas pressure, baking time) are not critical. As a result of this procedure, the graphite bonds very efficiently onto the metal: in the present case, the copper foils, but also onto the stainless steel (this explains the use of Grafoil to protect the sample). This process seems to be due to a fast surface diffusion and adhesion. This technique has been communicated to other groups, and similar results have been obtained using different metals.<sup>7</sup>

#### D. Magnetic-field coils

A superconducting coil located in the vacuum can and wound on the thermal shield at the still temperature provides the magnetic field required by the NMR experiment (273.16 G). The specially designed high-stability power supply is modulated by an external signal (generated by the computer) to provide a magnetic-field sweep. Superconducting coils at 4.2 K allow one to apply a magnetic-field gradient on the sample to improve the main field homogeneity. The residual gradient over the sample region is smaller than  $0.01\ \text{G}/\text{cm}$ .

### E. Thermometry

The CMN thermometer located inside the mixing chamber provided the temperature at zero magnetic field. The powdered CMN was obtained by grinding freshly grown single crystals, and packed to form a cylinder (diameter equal to height, 5 mm). The CMN mass was 0.146 g. It was located in an Araldite form where the primary and an astatic pair secondary were wound with superconducting wire. A mutual inductance bridge (Barras-Provence) designed in our laboratory was used to measure the CMN susceptibility with a precision better than 1 in  $10^5$  in all the temperature range. We shall see that other factors will degrade this accuracy.

This thermometer was calibrated (at zero magnetic field) between 1 and 2 K against the vapor pressure of the  $^4\text{He}$  bath, and the superconducting fixed point device SRM 767 of the National Bureau of Standards. The measured mutual inductance  $M$  followed the law  $M - M_0 = A/T^*$  within 0.5% in the calibration range. The constant term  $M_0$  results from the diamagnetic contribution of the CMN, the imperfect cancellation of the astatic pairs, and an offset of the inductance bridge chosen to cancel approximately the previous contributions.  $T^*$  is the "magnetic temperature:"  $T^* = T - \Delta$ . We have found in previous experiments, where the CMN thermometer was compared to the nuclear susceptibility of platinum, a value of  $\Delta = +0.25$  mK. This gives an estimation of the deviations from the CMN Curie law that can be expected.

Abraham, Ketterson, and Roach<sup>16</sup> suggested the use of CMN for secondary thermometry in the presence of a magnetic field: the smallness of the field dependence of the perpendicular component of the susceptibility tensor provides a useful temperature variation of the susceptibility. The following procedure was adopted here: the zero-field susceptibility of CMN was measured after complete stabilization of the refrigerator; the field was then raised to the final value of 273.16 G in about 10 min, causing a transient heating of the CMN; when the equilibrium was reached, the value of the mutual inductance under field was determined. The field was then reduced to zero to allow for a check of the stability during the procedure. This is rather straightforward above 10 mK, where time constants are relatively small. The uncertainties on the temperature in this range are smaller than 1%. Below 10 mK the CMN thermal time constant becomes larger than 1 h and the uncertainty on the temperature raises to 2% at the lowest temperature. The sensitivity to temperature changes in the CMN is much better than 0.1%.

Our calibration of the CMN mutual inductance under 273.16 G is shown in Fig. 2. The constant term  $M_0$  has been subtracted from the mutual inductance; its value was found to depend very slightly on the magnetic field. The main effects are a reduction of the effective Curie constant and a partial saturation at the lowest temperatures due to the anisotropy of the  $g$  factor and the powder average. Detailed investigations of this behavior are in progress.

To our knowledge, this is the first time that CMN thermometry under field is used in the range 3 mK–1 K; the

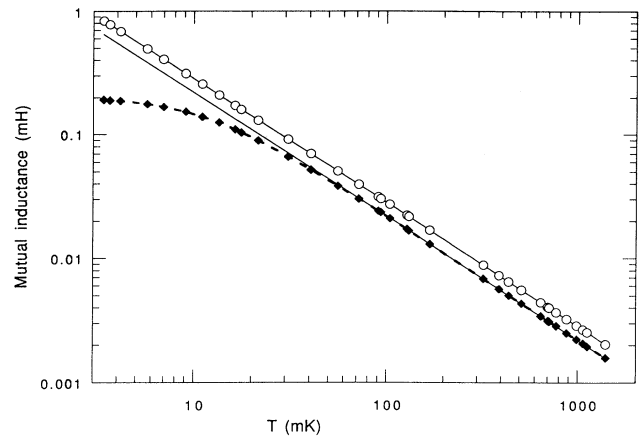


FIG. 2. CMN mutual inductance thermometer: calibration at zero field (open circles) and under a magnetic field of 273.16 G (diamonds). Constant terms have been subtracted (see text).

long-term reproducibility and high sensitivity of the usual zero-field CMN thermometry are essentially preserved, as well as the simplicity of the operation once calibrated.

Several calibrated carbon resistors were also used for control: a Matsushita 68 $\Omega$  was located on the copper post inside the experimental cell; a Speer 100 $\Omega$  and an Allen Bradley 100 $\Omega$  were immersed in the liquid of the mixing chamber. The latter was used in the temperature range 4–10 K to control the annealing procedure. The other resistors were calibrated below 4 K down to 3 mK. Saturation effects became large below 5 mK; practical use is limited to a temperature range 15 mK–4 K due to long time constants (several hours) at the lowest temperatures. A Barras-Provence PIO resistance bridge designed in our laboratory was used for the carbon resistance measurements. The temperature of the dilution refrigerator was controlled by a heater located on the concentrated side of the connecting tubes 10 cm apart from the mixing chamber, to avoid internal thermal gradients. For the same reason, the phase boundary was located near the top of the mixing chamber, away from the experimental cell region.

### F. The NMR spectrometer

The  $^3\text{He}$  NMR signals were measured with a high sensitivity and very low power CW spectrometer working as a rf bridge<sup>17</sup> (Fig. 3). We used a Fluke 6060A synthesizer to generate rf at 886 KHz with an excellent amplitude stability. The sample NMR coil (inductance  $\sim 100 \mu\text{H}$ ) was part of a parallel resonant circuit ( $Q = 44$ ) which was fed through an attenuator and a capacitor. The rf voltage on the resonant circuit was amplified by a high impedance differential preamplifier. A signal from the same generator and conveniently dephased was fed to the second input of the preamplifier to minimize the output, since only variations of the rf voltage are of interest.

The resulting rf signal was sent to a PAR 5202 high-frequency lock-in amplifier. Typical voltages on the rf coil were in the range 0.2–10-mV rms. The preamplifier gain was 100, and the compensation between the differential inputs on the order of 1%. The signal at the

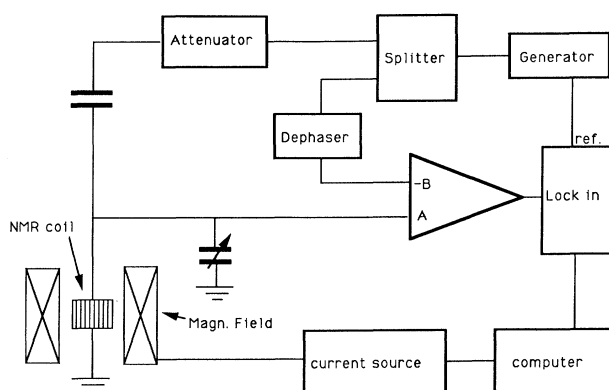


FIG. 3. Diagram of the NMR spectrometer.

lock-in was therefore in the mV range. The NMR absorption signal observed by sweeping the field around 273.16 G had an amplitude of the order of  $10\ \mu\text{V}$  at the rf coil with one monolayer of adsorbed  $^3\text{He}$  at 20 mK. Under these conditions the signal-to-noise ratio was better than  $10^3$ . This figure does not improve at lower temperatures, since the increase in the susceptibility is compensated by the smaller rf voltage required by thermal equilibrium limitations. At 100 mK, the signal-to-noise ratio is on the order of 100. The quality factor  $Q$  of the NMR coil is mainly determined by losses in the Grafoil. The variation of the electrical conductivity<sup>18</sup> due to quantum localization effects is fortunately small enough to consider that  $Q$  is essentially constant in this experiment. Another possible source of variation of  $Q$  is the change of the coaxial lines resistance with temperature; we checked for this effect by measuring the voltage on the circuit at resonance and varying the temperature. The overall stability of the NMR spectrometer was better than 1% over a 1-yr period.

A microcomputer was used to control the magnetic-field sweep and to measure the output of the NMR spectrometer. A calibrated attenuator (0.2%) used as an amplitude reference for the absorption signal was commanded through a digital output. 280 measurements of the rf signal were performed during the field sweep. The resulting digitalized NMR line, together with a detailed record of the data parameters, temperature, coverage, frequency, rf voltage, spectrometer setting, was then sent to a VAX-11/780 computer for storage on magnetic tape and data processing. This was necessary to handle more than 1500 NMR lines measured in this experiment.

### G. Thermal equilibrium and rf heating

The main problem in this experiment is to cool the Grafoil substrate, one of the worst materials from the point of view of its thermal conductivity.<sup>19</sup> The sintering technique used to attach each Grafoil piece to copper foils allowed us to cool the sample down to the lowest temperatures reached by the refrigerator, as evidenced by the susceptibility measurements in the high density solid (see Sec. IV). A test was performed at different temperatures to determine the maximum rf power level which

caused a reduction of the susceptibility (within 1%) by heating or saturation of the NMR line. We found no evidence of any coverage dependence of this maximum power. Grafoil is not a good electrical conductor, but eddy current losses must be taken into account: the quality factor of the resonance coil is essentially determined by the losses in the Grafoil. In practice, the maximum rf power that could be dissipated in the Grafoil during the measurements was in the range  $10^{-12}$ – $10^{-9}$  W depending on the temperature. This agrees within 1 order of magnitude with an estimation based on the thermal conductivity of Grafoil, the electrical characteristics of the circuit, and a simple model of uniform heating and conduction to the copper foils.

Care was taken to ensure that all other sources of power were well below picowatt levels. This was the main reason to locate the cell inside the mixing chamber. We avoided rf leakage through the electrical wires by a specially designed system of filters at room temperature and in the bath at 4.2 K; the contribution of this source of noise is below  $10^{-15}$  W, measured by GaAs detectors.

Eddy current heating due the magnetic-field sweep was minimized by using plastic components when possible, and by reducing the area of metallic parts normal to the field. The Grafoil and copper foils were therefore oriented with the normal to the planes perpendicular to the static and to the rf field. With the magnetic-field sweep rate of 0.018 G/sec used in this experiment, no eddy current heating was detected within the spectrometer resolution (sweeping the field at different rates or keeping the sweep on for a long period did not decrease the NMR signal).

### H. Adsorption isotherms and “commensurate” coverage scale

The  $^3\text{He}$  adsorption isotherms were determined at 4.20 K using a 100-Torr MKS Baratron pressure meter. Gas was admitted to the cell from a calibrated volume of 24.9  $\text{cm}^3$ . The adsorbed volume was calculated subtracting from the total amount of gas introduced in the system the amount which remained in the gas phase:  $(1.93 \pm 0.1) \cdot P[\text{cm}^3 \text{ STP}]$ , where  $P$  is the pressure in Torr. The resulting adsorption isotherm is shown in Fig. 4 and compared with those measured by Bretz *et al.*<sup>6</sup> and Goellner, Daunt, and Lerner.<sup>20</sup> They have been normalized at 1 Torr, i.e., a convenient pressure near monolayer completion where thermomolecular and nonadsorbed gas corrections are small. The excellent agreement indicates that nonadsorbed gas corrections are within our estimated error bars.

The commonly used  $A$  or  $B$  points<sup>6,9</sup> are not well defined when measuring with high precision: the slope changes continuously. (The  $A$  point is defined by the extrapolation of a linear portion of the isotherm to  $P=0$ , and the point  $B$  is defined as the point where the isotherm departs from a linear behavior at low pressures.) Forcing a linear fit between 1 and 5 Torr (a usual range) gives a  $B$  point monolayer determination of  $(23 \pm 1) \text{ cm}^3 \text{ STP}$ . This large uncertainty comes from the lack of any sharp feature in the adsorption isotherm corresponding to monolayer coverage, although the adsorption isotherm is very sensitive to coverage variations. This suggests a

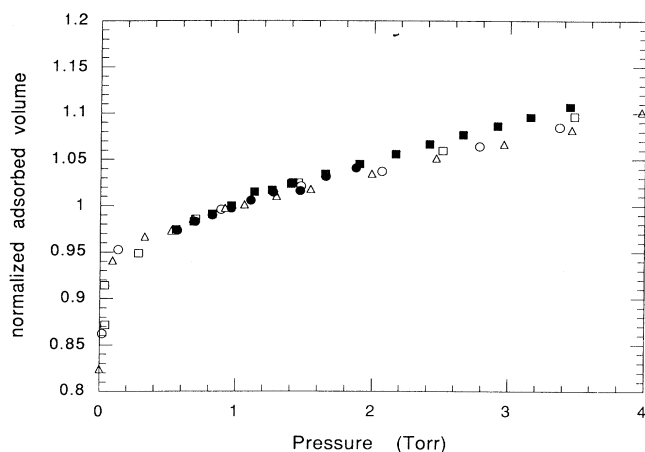


FIG. 4.  $^3\text{He}$  adsorption isotherms on Grafoil at 4.2 K (Ref. 6, cell A: open circles; cell B: open squares; Ref. 20: open triangles; this work, adsorption: solid squares; desorption: solid circles). The adsorbed volume has been normalized to that adsorbed at a pressure of 1 Torr.

better way to relate the adsorbed volumes to the areal density of the adsorbed  $^3\text{He}$ , combining the high precision of the adsorption isotherms and specific-heat determinations of the registered phase coverage. Bretz *et al.*<sup>6</sup> give the adsorbed volume at the registered phase (theoretical areal density  $n_c = 0.06366$  atoms/ $\text{\AA}^2$ ) and the adsorption isotherm on the same sample. From the scaling of the isotherms shown in Fig. 4, we determine the adsorbed volume at the registered phase density in our experiment to be  $(13.24 \pm 0.1)$  cm<sup>3</sup> STP. Therefore, the area of the sample is  $A_c = (55.9 \pm 0.4)$  m<sup>2</sup>. The index “c” is used to remind one that the area determination, and hence the coverage scale, is based on the commensurate phase.

According to Bretz *et al.*<sup>6</sup> promotion of atoms to the second layer begins at  $0.108$  atoms/ $\text{\AA}^2$ , and hence, in this experiment, to  $(22.4 \pm 0.3)$  cm<sup>3</sup> STP. This defines “the monolayer” ( $X = 1$  layer), used in this paper as a unit of coverage (the validity of this coverage scale will be discussed in detail later).

### I. Sample preparation

The sample cell was flushed with  $^3\text{He}$  gas and pumped for several days at room temperature with a nitrogen-trapped diffusion pump. The system was then cooled down to 4.2 K and remained below this temperature throughout the whole experiment, except during the annealing procedure.

Pure  $^3\text{He}$  ( $< 100$  ppm of  $^4\text{He}$ ) was admitted into the calibrated volume of the gas handling system through a charcoal trap kept at liquid-nitrogen temperature. Monolayer coverage corresponds to about 700 Torr in the calibrated volume at room temperature. Coverage variations were typically on the order of 5% of a monolayer, and the measured pressures around 30 Torr. The use of the 100-Torr Baratron gauge ensures that the uncertainty in the pressure measurements is much smaller than 1%.

The gas was introduced in the cell at 4.2 K to avoid condensation on cold spots of the filling capillary. Exchange gas (1 Torr of He) in the vacuum can and the dilution unit ensured thermal equilibrium. The exchange gas was pumped and the cell was heated up to 8 K to anneal the adsorbed  $^3\text{He}$ . After several hours the cell was allowed to cool down overnight to 4.2 K. The cell was then cooled down to 0.7 K by circulating a small amount of mixture in the refrigerator, also keeping the  $^4\text{He}$  pot temperature above the cell temperature. The purpose of this procedure ensured that all the gas would be adsorbed in the cell. At this point the normal operation of the refrigerator was started. Cooling the cell down to 3 mK required 24 h.

## IV. SUSCEPTIBILITY MEASUREMENTS

### A. Method of measurement

The area of the NMR adsorption signal is proportional to the nuclear susceptibility of the  $^3\text{He}$  spins.<sup>21</sup> It is necessary to sweep the field far away from the resonance peak to obtain a well-defined base line, but it is necessary to have a good resolution near the line center to measure the absorption signal with precision. The optimum magnetic-field sweep amplitude was determined at each coverage by a measurement of the area of the absorption signal as a function of the sweep amplitude. The minimum sweep which guaranteed a loss of area of the signal smaller than 2% was chosen as the operation sweep. Data were subsequently corrected for this effect. Typical sweep amplitudes of about 30 times the linewidth were found necessary.

The spectrometer provides a NMR line digitized to 280 points. The first and last 40 points were used to define the base line which, because of the good spectrometer stability, was a straight line with zero slope. The area between the fitted base line and the measured NMR line was calculated numerically, normalized in amplitude by the signal from the calibrated reference attenuator. The resulting figure is proportional to the susceptibility, with a scaling factor which is independent of the field sweep and of the spectrometer setting rf level, amplifier gain, etc.). We shall call it hereafter “the susceptibility” (in arbitrary units), following the usual designation. This magnitude is proportional to the number of spins per unit volume, and hence, in our system, per unit area. Note that the susceptibility is the area *measured* under the NMR line, and not the area obtained from a fit assuming a particular line shape. This would result in substantial systematic errors, due to the strong variation of the line shape with coverage discussed in Sec. IV D.

### B. Background

A background signal (due to the  $^3\text{He}$  from the mixing chamber seen by the NMR coil) was observed, despite the fact that a rather large cell (compared to the Grafoil sample size) was used in this experiment. The background signal was measured before the introduction of  $^3\text{He}$  samples in the experimental cell. It was small and constant

at low temperatures, with a slight decrease above 150 mK, as a consequence of Fermi degeneracy effects combined with the temperature dependence of the equilibrium concentration of the mixture. The background has been subtracted from all the data, which correspond therefore only to the  $^3\text{He}$  spins in the sample cell. The correction is on the order of 8% at 20 mK; this causes a maximum uncertainty on the order of 1% below this temperature. This correction increases to 20% at 300 mK, and few results in this temperature range will be reported here. Above 800 mK the refrigerator was operated with  $^4\text{He}$  circulation, and therefore no background was present in these measurements; this allowed susceptibility measurements up to 1 K where the uncertainty raises again to 10% due to the reduced signal.

### C. Susceptibility measurements as a function of coverage and temperature

The measurements were performed for 15 coverages:  $X = 0.531, 0.584, 0.637, 0.676, 0.722, 0.743, 0.810, 0.860, 0.910, 0.950, 0.990, 1.039, 1.128, 1.250,$  and  $1.450$  layers. The susceptibility was measured as a function of temperature between 2.8 mK and 1 K, with emphasis in the low-temperature region (below 30 mK).

Three main regions of coverage will be considered. The first, which covers the range 0.5–0.8 layers, contains the registered phase, the coexistence phase(s), and the low-density incommensurate solid. Previous NMR measurements indicate that exchange frequencies<sup>10,22</sup> in this region are larger than 1 MHz and effects larger than 0.1 mK were expected to show up in the susceptibility as Curie-Weiss terms. The second region, between 0.8 and 0.99 layers, corresponds to a dense incommensurate solid with very small exchange frequencies<sup>6,7,10,13,22</sup> and no measurable deviations from the Curie law can be expected here. The third coverage range, from 1 to 1.5 layers, corresponds to the beginning of second-layer promotion and formation of the second-layer fluid. Interlayer exchange and quantum degeneracy effects can be expected here. Obviously the first and last coverage regions are of interest. The second one, nevertheless, has been carefully measured since it provides a convenient way to check the reproducibility of the results and the calibration of the thermometers and the coverage scale. For that reason, these results are described first.

#### 1. Coverages between 0.8 and 0.99 layers (calibrations)

(a) Temperature calibration. The measured susceptibility at each coverage is well described by the expression  $\chi = C/(T^* + B)$ , where  $T^*$  is the magnetic temperature of the CMN at zero field and  $C$  is the Curie constant of  $^3\text{He}$ . As explained before, no deviation from a Curie law is expected here, and we consider  $B$  to be the Curie-Weiss temperature  $\Delta$  of the CMN itself. The uncertainty on  $B$  was found to be of the order of 0.05 mK at each coverage. No systematic variation of  $B$  was found in this range, as expected. Therefore,  $\Delta$  was taken as the average value of  $B$ :  $\Delta = (0.24 \pm 0.03)$  mK; the observed value agrees well with our previous determination of  $\Delta$  (see Sec. III E). In the following, all temperatures quoted have

been corrected by this factor:  $T = T^* + \Delta$ .

(b) Susceptibility calibration. The Curie constant  $C$  is linear in coverage: all the adsorbed  $^3\text{He}$  spins are affected by the NMR coil in this coverage and temperature range, and  $C = C_T$ , the Curie constant of all the  $^3\text{He}$  spins in the system:

$$C = C_T = Nc = nA_C c = C_0 X, \quad (1)$$

where  $N$  is the total number of  $^3\text{He}$  atoms,  $c$  the Curie constant per atom,  $n$  the areal density of  $^3\text{He}$  atoms,  $X$  the coverage expressed in layers, and  $A_C$  the substrate area (see Sec. III H).  $C_0$  is the “monolayer” ( $X=1$ ,  $n=0.108$  atoms/ $\text{\AA}^2$ ) Curie constant.

The measurements determine  $C_0 = (126.1 \pm 1)$  and therefore  $c = (20.9 \pm 0.3)10^{-20}$  expressed in our arbitrary units of susceptibility. This allows an absolute calibration of the susceptibility scale, since the number of  $^3\text{He}$  atoms and the magnetic moment of  $^3\text{He}$  are precisely known. The arb. units will be used throughout the paper since only relative values of the susceptibility are important.

#### 2. Other coverages below one layer (measurements)

The results are shown in Fig. 5 (using the corrected temperature scale) as a plot of  $\chi T/C_T$  vs  $1/T$  to em-

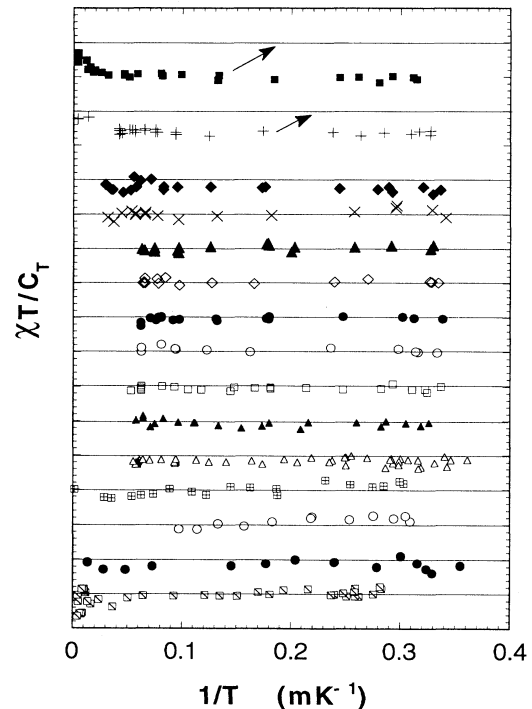


FIG. 5. Susceptibility ( $\chi$ ) results as a function of temperature ( $T$ ) and coverage ( $X$ ).  $C_T$  is the Curie constant for all the  $^3\text{He}$  spins in the cell at each coverage. The horizontal lines (data for different coverages have been shifted vertically to avoid superposition) correspond to  $\chi T/C_T = 1$  for each coverage (free-spin behavior). The shift is 0.1 for low coverages, and 0.2 for the last two coverages. Coverages, from bottom to top:  $X = 0.531, 0.584, 0.637, 0.676, 0.722, 0.743, 0.810, 0.860, 0.910, 0.950, 0.990, 1.039, 1.128, 1.250,$  and  $1.450$  atomic layers, as defined in the text.

phasize departures from the Curie law corresponding to a free-spin behavior. Clearly, in all this coverage range the deviations are extremely small, and the data are well fitted by the expression  $\chi = C/(T - \theta)$ . The Curie constant  $C$  as a function of coverage is shown in Fig. 6 and (normalized by the product  $C_0 X$ ) in Fig. 7.  $C$  is almost linear in coverage below one layer, close to the line  $C = C_0 X$  determined previously. For all coverages below the incommensurate phase a small (5%) systematic reduction of the Curie constant is seen. Since we performed measurements at higher coverages (before and after these measurements) finding the same spectrometer calibration, we believe that this effect is not due to an experimental artifact.

The Curie-Weiss temperatures  $\theta$  are shown in Fig. 8. In the incommensurate phase there is practically no departure from a free-spin behavior within our sensitivity on  $\theta$ , better than 0.12 mK.

In previous experiments at higher coverages (around two layers) we were able to observe large magnetic effects and to determine the sign of the exchange (ferromagnetic or antiferromagnetic depending on coverage); here, a slight *antiferromagnetic* tendency seems to be present as the coverage is reduced within the incommensurate phase, but this effect is close to the error bars.

At coverages around perfect commensurability, however, we observe *ferromagnetic* Curie-Weiss temperatures of about 0.25 mK. At registry density and at densities slightly below the incommensurate phase, the deviations from free-spin behavior were too small to be detected.

### 3. Coverages above one layer

Above one monolayer the Curie constant saturates progressively, indicating a substantial compression of the first layer and the formation of a degenerate liquid second layer. In this coverage range the data were fitted by the expression

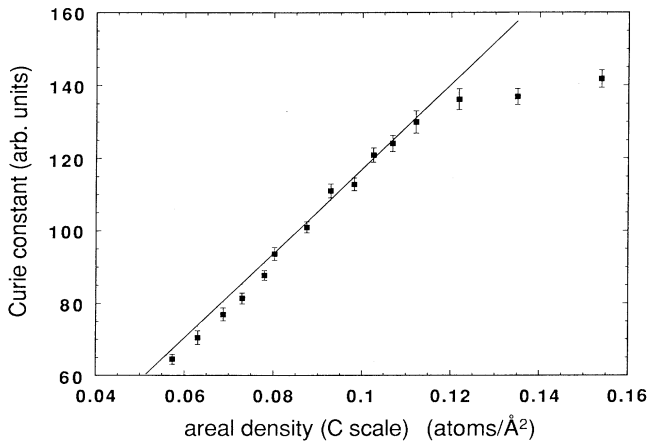


FIG. 6. The Curie constant  $C$  of the solid fraction as a function of coverage (solid squares). The total Curie constant  $C_T$ , determined by data in the incommensurate phase, is indicated by a straight line. The  $C$  coverage scale (see text) is based on the results of Ref. 6 and the adsorption isotherms shown in Fig. 4.

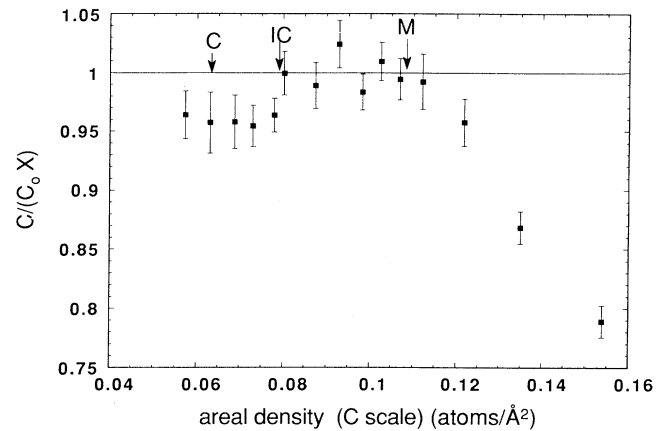


FIG. 7. The Curie constant  $C$  normalized by its value  $C_0$  at the “monolayer” ( $X = 1$ , areal density  $n = 0.108$  atoms/Å<sup>2</sup>) and by the coverage  $X$ , to emphasize departures from free-spin behavior. The arrows mark the commensurate phase ( $C$ ), the beginning of the incommensurate phase, and beginning of second-layer promotion (monolayer completion,  $M$ ), according to Ref. 6.

$$\chi = N_S c / (T - \theta) + (N_L c / T_F^{**}) [1 - \exp(-T_F^{**}/T)] \quad (2)$$

corresponding to  $N_S$  spins in a solid phase and  $N_L$  spins in a 2D Fermi-liquid phase;  $c$  is the Curie constant per atom (see above), and  $T_F^{**}$  an effective Fermi temperature. The Curie-Weiss temperatures  $\theta$  of the solid fraction were found to be smaller than 0.15 mK in this coverage range.

The expression above has been used with success to describe <sup>3</sup>He films on graphite preplated with <sup>4</sup>He.<sup>12</sup> In our experiment, however, the first layer is a solid <sup>3</sup>He layer which gives a very large contribution: its Curie constant  $C = cN_S$  is 136.9 arb. units for  $X = 1.250$ . This value is indeed surprising: using the sample area determined above and formula (1), the first (solid) layer density would be  $n_S = 0.117$  atoms/Å<sup>2</sup>, much larger than that determined directly by neutron scattering<sup>5</sup> (0.107 atoms/Å<sup>2</sup> at this coverage). That is, the signal from the dense first layer corresponds to more atoms than expected.

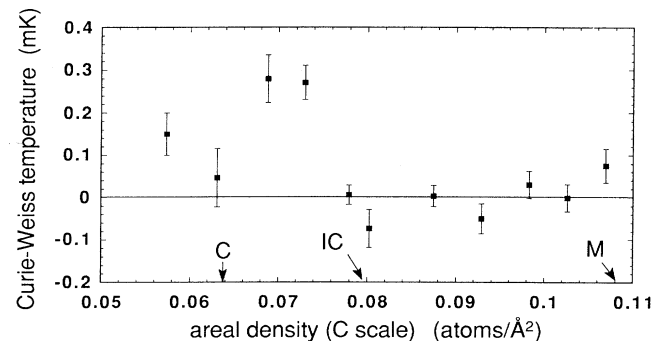


FIG. 8. Curie-Weiss temperatures determined at submonolayer coverages as a function of coverage (see caption of Fig. 7).

#### 4. The incommensurate scale of coverage

Recent neutron data<sup>5</sup> also show such a large discrepancy: if one assigns the density of the commensurate phase ( $0.063\,66\text{ atoms}/\text{\AA}^2$ ) to the amount of gas  $V_c$  yielding the best diffraction peak within the commensurate phase, then the measured lattice parameters within the incommensurate phase correspond to areal densities substantially smaller than those expected from the amount of adsorbed gas, as seen in Fig. 9. That is, the area available for adsorption seems to grow as the coverage increases, due either to a reduced fraction of a pure commensurate phase or to a progressive occupation of nonbasal planes of the graphite substrate.

A different coverage scale must be used in the incommensurate phase if indeed the area  $A_I$  is larger than that determined in the commensurate phase ( $A_C$ ): the “incommensurate” coverage scale ( $I$  scale; coverages noted as “ $n_I$ ”). The proportionality factor between the Curie constant and the areal density is different in the  $I$  scale, due to the different area:

$$C = Nc = n_I A_I c = n A_C c . \quad (3)$$

There is no reason *a priori* to use for our Grafoil substrate the area enhancement factor determined by neutron scattering on a ZYX graphite sample. However, it is possible to calibrate the area  $A_I$  of our sample by comparing neutron data and ours above monolayer completion. The procedure is the following: neutron-scattering data show that the first-layer density is almost constant and equal to  $n_I = 0.107\text{ atoms}/\text{\AA}^2$  in a relatively large coverage range above monolayer completion, around  $X = 1.25$ . Hence, the measured Curie constant  $C = 136.9\text{ arb. units}$

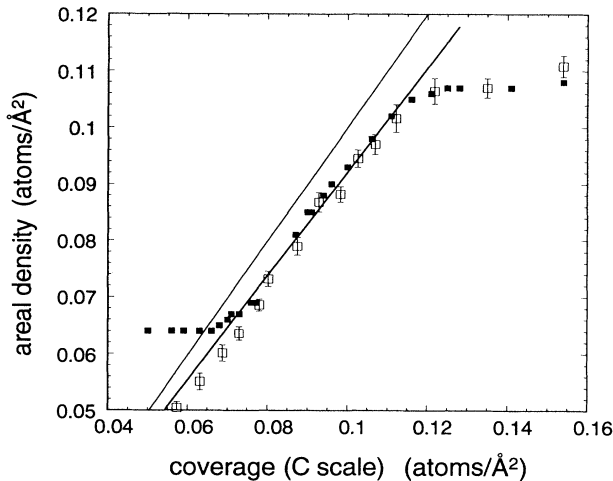


FIG. 9. Areal density determined by neutron scattering (Ref. 5) (solid squares), and by present measurements (Curie constant normalized to obtain the incommensurate scale as described in the text) (open squares) as a function of the coverage expressed in the commensurate coverage scale. The measured densities differ substantially from the  $C$  scale values in this coverage range: equal values would be given by the upper straight line. NMR and neutron data agree well at all coverages within the incommensurate phase. The thick line passes through the origin; it corresponds to free-spin behavior for the NMR data.

for the first layer at our total coverage  $X = 1.250$  should correspond to  $n_I = 0.107\text{ atoms}/\text{\AA}^2$ , instead of the value  $n = 0.117\text{ atoms}/\text{\AA}^2$  found previously using the “commensurate coverage scale ( $C$  scale).” The effective area for the incommensurate phase is then  $A_I = (61.2 \pm 0.4)\text{ m}^2$  compared to  $A_C = (55.9 \pm 0.4)\text{ m}^2$  for the commensurate phase.

This is a large effect: coverages change by 9.5% (see Table I). The ratio between the coverage scales determined by neutron scattering (on a different sample, ZYX exfoliated graphite) using coverages below second layer promotion is 8.5%. That is, both experiments indicate an increase on the order of 9% of the effective area. Both sets of data are shown in Fig. 9: the direct areal density measurement by neutron scattering, and the areal density determined from our Curie constant with the incommensurate coverage scale; both sets of data are plotted as a function of the amount of adsorbed gas measured with the commensurate coverage scale. Clearly, the agreement is good in the incommensurate phase below monolayer completion, for the rounding near the monolayer completion, and obviously above monolayer completion since the calibration with neutron data was performed there.

At our highest coverage, however, a small and unexpected increase of the Curie constant is seen, which could indicate the growth of a small amount of solid in the second layer, even before the coexistence region identified by specific heat.

#### 5. Second-layer fluid

The susceptibility of the second-layer fluid is determined as described in Sec. IV C 3, as a function of density. The results are compared to those obtained on a related system (second-layer  $^3\text{He}$  fluid, but on a  $^4\text{He}$  preplated graphite substrate<sup>12</sup>). Obviously, error bars are much larger here due to the subtraction of the large first-layer contribution. As seen in Fig. 10, we find similar

TABLE I.  $^3\text{He}$  coverages investigated in this work, expressed in layers ( $X$ ), in the commensurate coverage scale ( $n_C$ ) and in the incommensurate coverage scale ( $n_I$ ) defined in the text.

$X$ (layers)	$n_C$ (atoms/ $\text{\AA}^2$ )	$n_I$ (atoms/ $\text{\AA}^2$ )
0.531	0.0573	0.0528
0.584	0.0630	0.0581
0.637	0.0688	0.0634
0.676	0.0730	0.0673
0.722	0.0780	0.0718
0.743	0.0802	0.0739
0.810	0.0875	0.0806
0.860	0.0929	0.0856
0.910	0.0983	0.0905
0.950	0.1026	0.0945
0.990	0.1069	0.0985
1.039	0.1122	0.1034
1.128	0.1218	0.1122
1.250	0.1350	0.1244
1.425	0.1539	0.1418

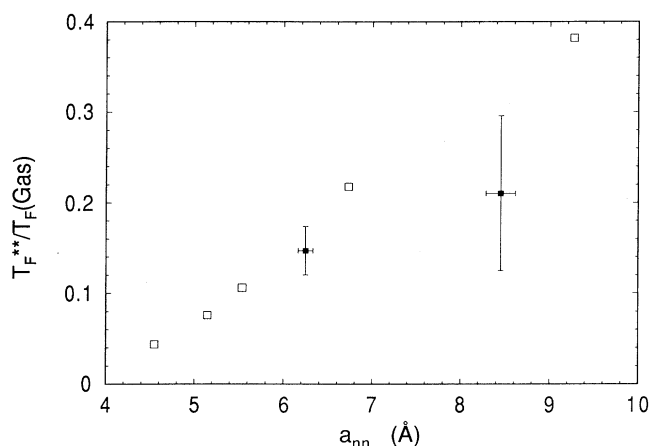


FIG. 10. Fermi temperature of the second-layer fluid (pure  $^3\text{He}$  film), normalized by that of the noninteracting system at the same density, as a function of the interparticle distance. Solid squares: present data. Open squares: data from Ref. 12 ( $^3\text{He}$  second-layer on a  $^4\text{He}$  first layer).

values for  $T_F^{**}$ , with a tendency toward smaller degeneracy temperatures. The values in Fig. 10 are normalized (see Ref. 7) by the Fermi temperature of the noninteracting Fermi gas ( $T_{F\text{ gas}}=50.5n$ ); the nearest-neighbor distance  $a_{\text{NN}}$  is obtained from the relation  $a_{\text{NN}}=1.075n^{-1/2}$ , where  $n$  is the second-layer density using the  $I$  scale of coverages.

### 6. Line shapes

The line shapes of adsorbed  $^3\text{He}$  have been studied by several authors. Hedge and Daunt<sup>14</sup> observed nearly Lorentzian lines and showed that their width ( $\approx 0.2$  G) is essentially determined by the Grafoil substrate diamagnetism. Pulsed NMR experiments<sup>13,23</sup> performed at Sussex and Tokyo have given results of the variation of  $T_2$  with coverage, which imply large motional narrowing effects except near the monolayer coverage, where the rigid lattice value for  $T_2$  is almost reached. This corresponds to a linewidth on the order of 1 G. Nevertheless, nearly Lorentzian line shapes were observed. Above monolayer coverage double exponential decay of the transverse sus-

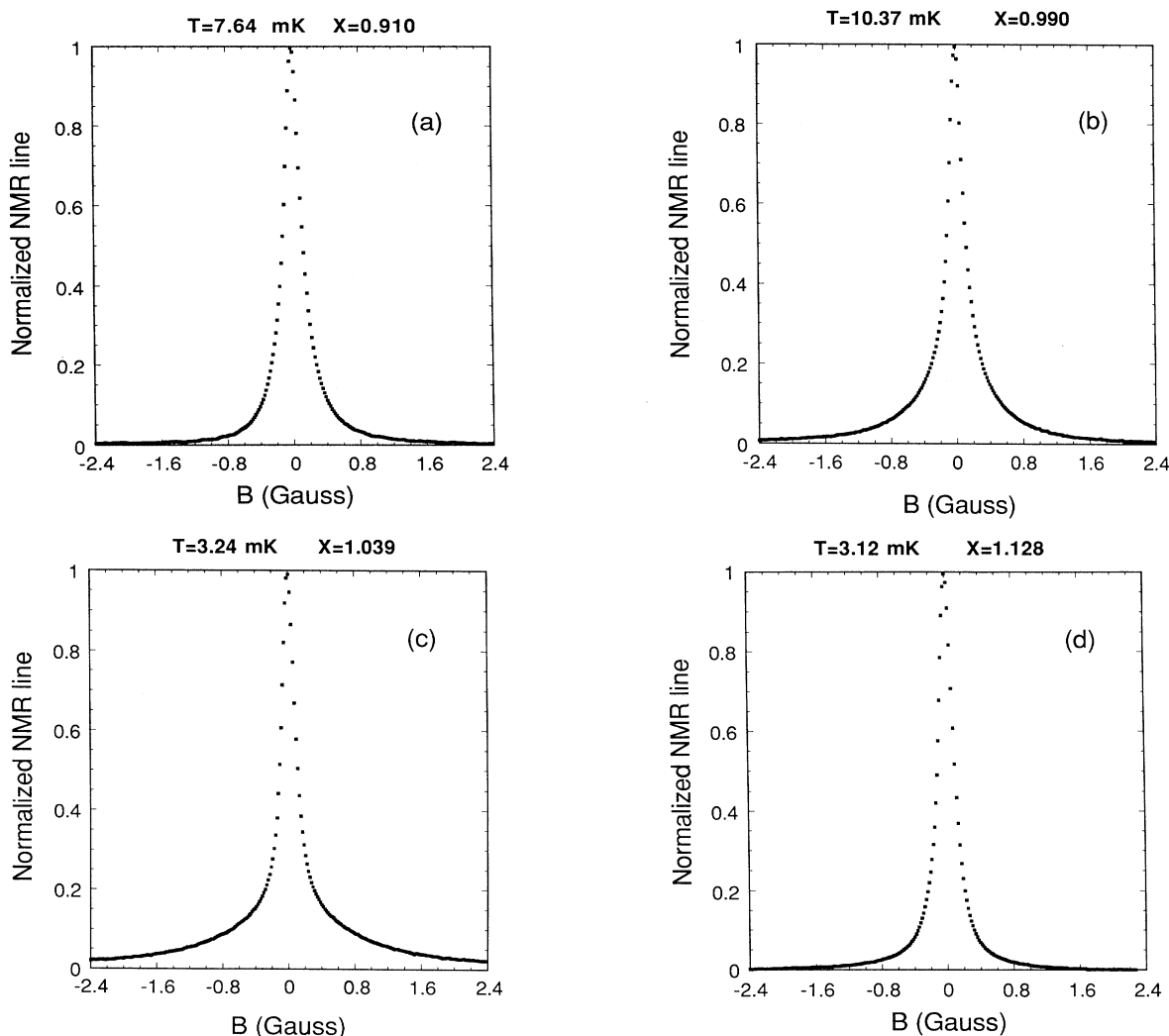


FIG. 11. NMR absorption lines at coverages around monolayer completion: (a)  $X=0.910$ , (b)  $X=0.990$ , (c)  $X=1.039$ , (d)  $X=1.128$ . Note the broadening and the development of non-Lorentzian line shapes, followed by an incomplete narrowing.

ceptibility has been reported,<sup>24</sup> i.e., the line shape consists of two Lorentzian lines with different widths. A cusp in  $T_2$  associated to this coverage region has been often used as a marker of monolayer completion.

The shape of the NMR line is not directly relevant for the susceptibility measurements. Nevertheless, it is worth mentioning some observed features which implied particular care in this experiment, and which are related to the coverage scales.

For coverages  $0.5 < X < 0.9$ , a good agreement with previous results<sup>14</sup> is obtained: a nearly perfect Lorentzian line with a Grafoil induced full width at half maximum (FWHM) broadening of 0.12 G added to the homogeneous linewidth. However, at  $X = 0.9$  the quality of the fit degrades, suggesting a change in the line shape.

For coverages  $0.9 < X \leq 1.039$  a broad component of the line develops clearly (Fig. 11). The lines can be fitted by two Lorentzians; the width of the narrow one corresponds practically to the Grafoil inhomogeneous broadening, whereas that of the broad component follows the naively expected behavior: it broadens as the density increases (the motional narrowing effect decreases), towards the rigid lattice value. Both Lorentzians have the same area (within 10%), independently of coverage within this range. Below  $X = 0.9$  the fit with two Lorentzians becomes uncertain, since both components have similar width. However, as seen in Fig. 12, one can reasonably consider that this behavior is present at least in a large fraction of the incommensurate phase. Other fits of the NMR line provide good results, like the "stretched Lorentzian"  $[(B/B_0)^{2\alpha} + 1]^{-1}$ , where  $B$  is the field,  $B_0$  a generalized linewidth, and  $\alpha$  an adjustable parameter  $\leq 1$ .

For the purpose of susceptibility measurements, the ex-

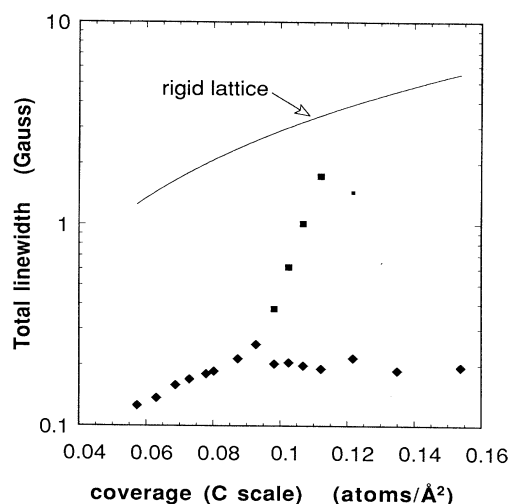


FIG. 12. Linewidth (FWHM) of the Lorentzian NMR lines as a function of coverage. Above  $n = 0.09$  atoms/Å<sup>2</sup>, fits with two-Lorentzians of approximately equal areas describe the data. The broad component (squares) evolves toward the rigid lattice value, whereas the narrow one is basically determined by the substrate diamagnetism. Above monolayer completion the intensity of the broad component is reduced (small square) and finally vanishes.

istence of a broad component implied that field sweeps of about 15 G were typical for coverages above 0.95 of a monolayer. It is important to note that the Lorentzian fit of the broad component, although satisfactory to determine the width, is very inaccurate to determine the area of the NMR line (fits overestimate the susceptibility by more than 20% around monolayer coverage): far from its center, the broad component decays faster than the Lorentzian fit, due to the natural cutoff of the rigid lattice dipolar interaction.

This behavior persists for coverages slightly above  $X = 1$ : at  $X = 1.039$  the broad component is almost 1 order of magnitude broader than the narrow one, and its amplitude is reduced in the same proportion. A qualitative change appears at higher coverages: at  $X = 1.128$  the narrow component grows at the expense of the broad component: the ratio of their areas becomes 10/1. Clearly, the liquid in the second layer is efficient to produce motional narrowing. At higher coverages, the line can be fitted with one narrow Lorentzian (width  $\approx 0.2$  G), but we cannot exclude the possibility of a broad second line (width  $\geq 2$  G) having  $\leq 2\%$  of the main line's height. Note that most of the intensity comes from the very dense first layer, and the line is nevertheless very narrow.

## V. DISCUSSION

The evolution of the Curie constant as a function of coverage (Figs. 6 and 7) displays several striking features. At all the coverages investigated here below the incommensurate phase coverage, a 5% reduction of the Curie constant is found. This effect can be seen directly in the susceptibility data shown in Fig. 5, and seems to be correlated to the presence of substrate-induced inhomogeneities in the adsorbed layer (see the comparison with neutron data, Fig. 9). This may indicate that a small fraction of the spins is degenerate (Fermi fluid) or that its NMR line is too broad to be detected (spins not participating to efficient exchange processes). A reduction of the Curie constant at low temperatures has been reported<sup>12</sup> for coverages below the commensurate phase coverage, interpreted as a degeneracy effect around defects. Our data, however, show that this effect persists above this coverage until, at the coverage where the incommensurate phase is formed, the Curie constant reaches the free-spin value. This anomalous behavior of the Curie constant at intermediate coverages may be due to adsorption on nonbasal planes or on nonuniform regions of the substrate. Heat-capacity data exclude the possible existence of a liquid fraction only in a narrow range very close to the perfect commensurate coverage, and are not inconsistent with this hypothesis.

An anomalous behavior of the susceptibility has been reported<sup>12</sup> for the coverage range around registry, but at much higher temperatures (around 100 mK). We show a comparison of these data with the present results in Fig. 13 (coverages around  $X = 0.65$ ). The increase of the susceptibility above free-spin values reported in Ref. 12 at a coverage  $X = 0.611$ , which seemed to confirm our earlier report of this effect,<sup>4</sup> does not follow the gradual increase observed as a function of  $1/T$  in our data. In the incommensurate phase, as seen in Fig. 14, a similar disagree-

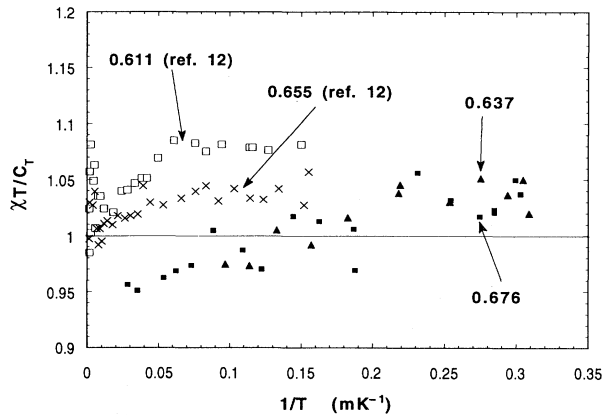


FIG. 13. Susceptibility data (normalized as in Fig. 5) as a function of the inverse temperature, for coverages slightly above the commensurate phase ( $X=0.589$  layers). Present data at  $X=0.637$  and  $0.676$ , and data from Ref. 12 at  $X=0.611$  and  $0.655$ .

ment is found. Therefore, two different problems are raised when comparing the data: a different temperature dependence at the lowest temperatures, and an anomalous behavior of the susceptibility at high temperatures. The origin of the discrepancies is unknown; it could be related to defects and annealing procedures (similar problems have been found<sup>7</sup> at low coverages), or to systematic errors handled differently in both experiments.

The Curie-Weiss temperatures  $\theta$  (Fig. 8) have been obtained assuming a pure Curie-Weiss behavior at the very low temperatures investigated here. The problems of the absolute value of the Curie constants discussed above may affect the determination of  $\theta$ . Nevertheless, the values found here place a very low upper limit to the exchange constants. Assuming a simple Heisenberg model, where  $\theta=3J$ , one deduces that exchange interactions are smaller than  $0.04$  mK in the incommensurate phase. This seems *a priori* inconsistent with high-temperature experiments, in particular, with the very careful analysis

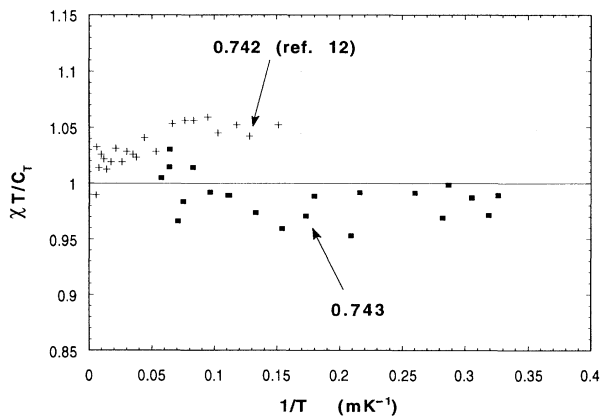


FIG. 14. Susceptibility data (normalized as in Fig. 5) as a function of the inverse temperature, for coverages within the incommensurate phase. Present data at  $X=0.743$ , and data from Ref. 12 at  $X=0.742$ .

of relaxation times performed by Cowan *et al.*<sup>22</sup> We show in Fig. 15 the exchange frequencies deduced using different techniques; note that we have modified the coverage scale of all data:<sup>25</sup> the  $I$  scale must be used in the incommensurate phase.

There is clearly a strong disagreement between all results. In a preliminary report of this effect<sup>4</sup> we suggested that this discrepancy is consistent with multiple-spin exchange: many exchange constants contribute to enhancing the nuclear relaxation, but strong cancellation effects reduce the Curie-Weiss temperature, expressed in this model as  $\theta=3(J_1+J_2+\dots+J_N)-2T+3K-5F+(\frac{5}{8})S$ , where the exchange coefficients correspond to  $N$ -neighbor two-particle exchange ( $J_N$ ), three- ( $T$ ), four- ( $K$ ), five- ( $F$ ), and six- ( $S$ ) particle exchanges.<sup>26</sup> Specific-heat measurements give intermediate values (Fig. 15), as expected from the combination of exchange constants in the multiple-spin exchange model, providing further support to this suggestion.

For coverages around the commensurate phase, a modest magnetic heat capacity was observed<sup>7</sup> at low temperatures, associated to an unusual  $1/T$  temperature dependence. Our measurements give a small value of the Curie temperature at the commensurate coverage, and a ferromagnetic tendency below and above this coverage (Fig. 8). This effect is qualitatively consistent with the heat-capacity data<sup>7</sup> at temperatures on the order of  $3$  mK (heat capacity does not give the sign of the exchange, however). Effects due to vacancies and defects around the commensurate phase are not surprising. Also, particular structures due to high-order commensurate phases on the graphite lattice can favor, by geometric effects, special types of cyclic exchanges; several overstructures have been proposed, but it is likely that few of these (except the canonical commensurate phase) can exist in a sizable coverage range. The experimental evidence is still

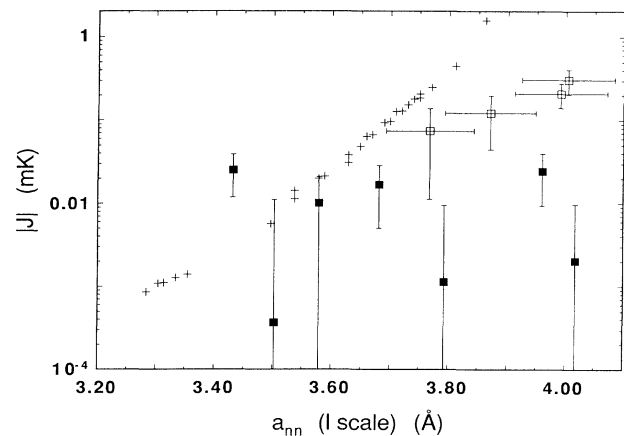


FIG. 15. Magnitude of the exchange constant within the incommensurate phase as a function of the lattice parameter, deduced from relaxation times (Ref. 22) (crosses), heat capacity (Ref. 7) (open squares), and present NMR susceptibility data (solid squares). The error bars on the abscissa of heat-capacity data indicate the uncertainty on the relative coverage scales (Ref. 25). This order-of-magnitude disagreement suggests the existence of multiple-spin exchange.

too limited to justify here a theoretical discussion<sup>26,27</sup> of the mechanisms leading to ferromagnetism in these phases.

The smallness of the nuclear exchange interactions at all submonolayer coverages, compared to values found in the second layer at similar areal densities, is due to the different adsorption potential in the third dimension (normal to the substrate), as shown by quantum Monte Carlo simulations:<sup>28</sup> particle exchange is not a strictly 2D problem.

The problem of coverage scales is particularly serious. The neutron-scattering and NMR results discussed above mean either that as much as 9% of the area of the graphite substrates (in principle, the best systems known presently) is heterogeneous and the “effective area” increases with coverage, or that the determination of the “commensurate phase coverage” is inadequate. It is also possible that unexplained errors affect some of the experiments. Heat-capacity, neutron-scattering, isotherms, and NMR provide information which is only partially overlapping. Further work is needed to establish a better coverage scale;  $^3\text{He}$  adsorption isotherms at 4.2 K are presently the simplest way to compare coverages between different experiments, but unfortunately their use is not generalized. The inaccuracy of the coverage scales has important consequences on the analysis of all the experiments performed up to now. Heat-capacity data, for instance, use the *C* scale; this may result in substantial errors in the densities within the incommensurate phase and at multilayer coverages, where a subtraction of the first-layer density is needed to determine second- and further layer densities.

The consequences of heterogeneity on the structural phase diagram of  $^3\text{He}$  (and other rare gases) adsorbed on graphite are simple to foresee; coexistence regimes involving parasitic phases may dominate in heat-capacity measurements, and to a smaller extent in NMR and neutron scattering. It is likely that the structure of the film at second-layer coverages (and hence its magnetic properties) will also be affected by a substrate heterogeneity.

Transverse relaxation time  $T_2$  measurements provide, in principle, an independent way to determine the commensurate coverage and the beginning of second-layer promotion.  $T_2$  minima have been reported and used for this purpose in the literature,<sup>13,22</sup> and continuous wave linewidth measurements were used recently to determine monolayer completion.<sup>12</sup> It is difficult to discuss in detail previous results based on  $T_2$  determinations, due to the lack of detailed information about the measured line shapes. Our data show clearly that two-Lorentzian lines (equivalent to two-exponential decays) are found at submonolayer coverages. Note that in  $T_2$  measurements lines as broad as those described here are difficult to detect. We have found that  $T_2$  data look similar to the values deduced from the inverse of the width of our lines taken at half high; the cusplike feature, however, is then found below one monolayer. The cusp in  $T_2$  occurs therefore at a coverage dependent on the sensitivity of the spectrometer, and is not very precise used as a monolayer marker. As an example, we show in Fig. 16 the linewidths determined in the present work (narrow and

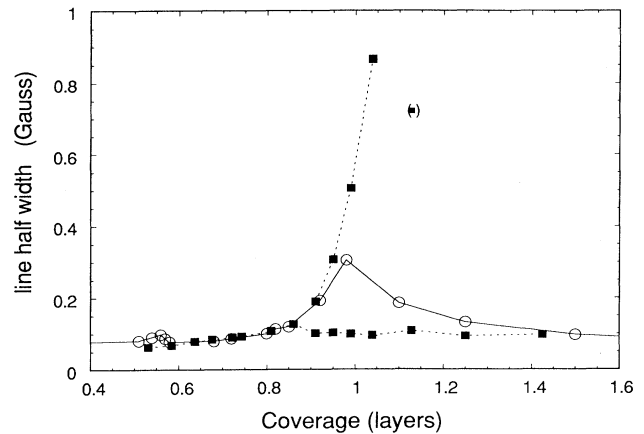


FIG. 16. Squares: CW NMR linewidth (HWHM) determined in the present work (see Fig. 12). Circles: values deduced from  $T_2$  data (Ref. 10) as explained in the text.

broad components) compared to the width deduced from  $T_2$  measurements<sup>10</sup> [the homogeneous Lorentzian line half width at half maximum (HWHM) is given (in G) by  $49/T_2$  if  $T_2$  is expressed in  $\mu\text{sec}$ ; an inhomogeneous broadening of 0.06 G has been added to give  $T_2^*$ ]. The effect discussed above is clearly seen around  $X=1$ . There is a good agreement below  $X=0.9$ , except in a small range around the commensurate phase: we do not see the broadening suggested by the  $T_2$  data. In recent CW line-shape measurements,<sup>12</sup> the inhomogeneous broadening was subtracted in an unspecified way. These linewidth data are found to be inconsistent with our own and previous  $T_2$  data at coverages  $0.5 < X < 0.7$ .

The two-Lorentzian lines have a very characteristic aspect: a narrow cusp and a very broad base. They are observed when the coverage is increased to values where the exchange frequencies become comparable to the dipolar width (see Fig. 15; 2 G corresponds to  $0.3 \mu\text{K}$ ), and therefore to an intermediate situation before reaching the Gaussian line shape. The two-Lorentzian fit is useful as an experimental tool to characterize the lines; the fact that both components have the same area independent on coverage suggests, however, that this is indeed a new line shape. This effect can be observed in this system because one can explore a very large range of interatomic distances without structural phase transitions.

Other interpretations of this unusual behavior of the NMR line shape are possible. For instance, it is well known that multiexponential decays are observed in molecular groups of similar atoms performing tunneling motions; we have therefore suggested<sup>4</sup> that multiple-spin exchange might lead to a similar behavior in this system. The line shapes can also be affected by hard-core effects, inhomogeneity of the 2D lattice (defects, corrugation of the layer, superstructures, etc). A detailed theory is presently lacking.

## VI. CONCLUSIONS

The effects of nuclear magnetic exchange in  $^3\text{He}$  adsorbed on Grafoil at submonolayer coverages are ex-

tremely small compared to those observed at multilayer coverages. An upper limit  $J \leq 40 \mu\text{K}$  is found in the incommensurate phase. Heat-capacity and relaxation time determinations of  $J$  provide different results (orders of magnitude), suggesting cancellation effects due to multiple-spin exchange, a situation already found in the 3D solid. At lower coverages, ferromagnetic deviations are observed both below and above the commensurate coverage; anomalies in the value of the Curie constant, probably associated with high-temperature effects<sup>12</sup> (around 100 mK), however, complicate the analysis in this coverage range.

Above monolayer completion, the coverage dependence of the Curie constant of the solid fraction is compared to recent neutron-scattering results. Both measurements indicate that present coverage scales, based on the determination of the commensurate phase coverage, may be in error by about 9%. This may be due to inhomogeneity of the graphite substrate, to an incorrect understanding of the commensurate phase, or to systematic errors in the experimental results.

The transition from Lorentzian line shapes to a different line shape (fitted approximately by two-Lorentzian lines, one of those having a width approaching the rigid lattice limit) is clearly observed in this sys-

tem. Narrowing of the line is observed above monolayer completion; the broad component disappears gradually, and hence this effect does not seem to be suitable to detect and calibrate monolayer coverages accurately.

Surface physics at very low temperatures has become quantitative due to the development of very sensitive and accurate techniques; the discrepancies pointed out here should help refining further measurements, and, in particular, contribute to the establishment of a coherent coverage scale, in order to understand the properties of two-dimensional quantum fluids and solids.

#### ACKNOWLEDGMENTS

We are grateful to H. J. Lauter for several years of fruitful collaboration, to W. G. Clark for teaching us CW NMR techniques, and to D. Ceperley, B. Cowan, D. S. Greywall, C. Lhuillier, M. Roger, J. Saunders, and O. Vilches for many valuable discussions and for communicating us their results prior to publication. We would also like to express our gratitude to the CNPq (Brazil), to the University of Grenoble, and to CNRS (France) for their financial support of this French-Brazilian collaboration.

- 
- <sup>1</sup>H. Franco, H. Godfrin, and D. Thoulouze, *Phys. Rev. B* **31**, 1699 (1985).
- <sup>2</sup>H. Franco, Thèse de Doctorat, Université de Grenoble, 1985; H. Franco, R. E. Rapp, and H. Godfrin, *Phys. Rev. Lett.* **57**, 1161 (1986).
- <sup>3</sup>H. Godfrin, R. R. Ruel, and D. D. Osheroff, *Phys. Rev. Lett.* **60**, 305 (1988), *J. Phys. (Paris) Colloq.* **49**, C8-2045 (1988).
- <sup>4</sup>H. Godfrin, *Can. J. Phys.* **65**, 1430 (1987); H. Godfrin, R. E. Rapp, and D. D. Osheroff, *Physica A* **163**, 101 (1990); H. Godfrin, R. E. Rapp, and H. J. Lauter, *Physica B* **169**, 177 (1991).
- <sup>5</sup>H. J. Lauter, H. Godfrin, V. L. P. Frank, and H. P. Schildberg, *Physica B* **165 & 166**, 597 (1990); H. J. Lauter, H. Godfrin, and P. Leiderer, in *Phase Transitions in Surface Films 2*, Vol. 267 of NATO Advanced Study Institute, Series B: Physics, edited by H. Taub *et al.* (Plenum, New York, 1991).
- <sup>6</sup>M. Bretz, J. G. Dash, D. C. Hickernell, E. O. McLean, and O. E. Vilches, *Phys. Rev. A* **8**, 1589 (1973); **9**, 2657 (1974); S. V. Hering, S. W. van Sciver, and O. E. Vilches, *J. Low Temp. Phys.* **25**, 793 (1976); S. W. van Sciver and O. E. Vilches, *Phys. Rev. B* **18**, 285 (1978).
- <sup>7</sup>D. S. Greywall and P. A. Busch, *Phys. Rev. Lett.* **62**, 1868 (1989); **65**, 2788 (1990); D. S. Greywall, *Phys. Rev. B* **41**, 1842 (1990).
- <sup>8</sup>M. Nielsen, J. P. McTague, and W. Ellenson, *J. Phys. (Paris) Colloq.* **38**, C4-10 (1977); R. Feile, H. Wiechert, and H. J. Lauter, *Phys. Rev. B* **25**, 3410 (1982); H. J. Lauter, H. P. Schildberg, H. Godfrin, H. Wiechert, and R. Haensel, *Can. J. Phys.* **65**, 1435 (1987).
- <sup>9</sup>J. G. Dash, *Films on Solid Surfaces* (Academic, New York, 1975).
- <sup>10</sup>M. G. Richards, in *Phase Transitions in Surface Films*, edited by J. G. Dash and J. Ruwals (Plenum, New York, 1980).
- <sup>11</sup>B. P. Cowan and A. J. Kent, *Phys. Lett.* **106A**, 54 (1984).
- <sup>12</sup>J. Saunders, C. P. Lusher, and B. P. Cowan, *Phys. Rev. Lett.* **64**, 2523 (1990).
- <sup>13</sup>J. R. Owers-Bradley, B. P. Cowan, M. G. Richards, and A. L. Thomson, *Phys. Lett.* **65A**, 424 (1978); B. P. Cowan, M. G. Richards, A. L. Thomson, and W. J. Mullin, *Phys. Rev. Lett.* **38**, 165 (1977).
- <sup>14</sup>S. E. Hegde and J. G. Daunt, *J. Low Temp. Phys.* **32**, 765 (1978), **34**, 233 (1979).
- <sup>15</sup>G. Frossati, H. Godfrin, B. Hébral, G. Schumacher, and D. Thoulouze, in *Proceedings of the Ultra Low Temperature Symposium, Hakoné, Japan, 1977*, edited by T. Sugawara, S. Nakajima, T. Ohtsuka, and T. Usui (Physical Society of Japan, Tokyo, 1978); G. Frossati, Thèse d'Etat, Université de Grenoble, 1978; H. Godfrin, Thèse d'Etat, Université de Grenoble, 1981.
- <sup>16</sup>B. M. Abraham, J. B. Ketterson, and P. R. Roach, *Phys. Rev. B* **6**, 4675 (1972).
- <sup>17</sup>The NMR spectrometer is based on a design due to W. G. Clark.
- <sup>18</sup>R. E. Rapp, L. D. Dillon, and H. Godfrin, *Cryogenics* **25**, 152 (1985).
- <sup>19</sup>L. D. Dillon, R. E. Rapp, and O. E. Vilches, *J. Low Temp. Phys.* **59**, 35 (1985).
- <sup>20</sup>G. J. Goellner, J. G. Daunt, and E. Lerner, *J. Low Temp. Phys.* **21**, 347 (1975).
- <sup>21</sup>A. Abragam, *The Principles of Nuclear Magnetism* (Clarendon, Oxford, 1961).
- <sup>22</sup>B. Cowan, L. Abou El-Nasr, M. Fardis, and A. Hussein, *Phys. Rev. Lett.* **58**, 2308 (1987).
- <sup>23</sup>K. Satoh and T. Sugawara, *J. Low Temp. Phys.* **38**, 37 (1980).
- <sup>24</sup>M. F. Secca and M. G. Richards, in *Proceedings of the 17th International Conference on Low Temperature Physics, Karlsruhe, 1984*, edited by U. Uckern, A. Schmid, W. Weber, and H. Wühl (North-Holland, Amsterdam, 1984), p. 741.

<sup>25</sup>The data of Ref. 22 were converted to the *C* scale by multiplying nominal densities by a factor 1.061, deduced from their unpublished adsorption isotherm. Greywall's data are based on the *C* scale with good accuracy (about 2%). Using the factor 1.09 (see text) between *C* scale and *I* scale densities, coverages were then converted to the *I* scale, to determine the nearest-neighbor distance  $a_{\text{NN}}$ .

<sup>26</sup>See M. Roger, *Physica B* **165 & 166**, 697 (1990); M. Roger, J. H. Hetherington, and J. M. Delrieu, *Rev. Mod. Phys.* **55**, 1 (1983); H. Godfrin and D. D. Osheroff, *Phys. Rev. B* **38**, 4492 (1988), and references therein.

<sup>27</sup>R. A. Guyer, *Phys. Rev. Lett.* **39**, 1091 (1977).

<sup>28</sup>D. Ceperley and C. Lhuillier (private communication).